JGR Space Physics

RESEARCH ARTICLE
10.1029/2022JA031118

# On Current Sheets and Associated Density Spikes in Titan's Ionosphere as Seen From Cassini

**Konstantin Kim[1,2], Niklas J. T. Edberg[1], Oleg Shebanits[1], Jan-Erik Wahlund[1], Erik Vigren[1], and Cesar Bertucci[3,4]**

[1]Swedish Institute of Space Physics, Uppsala, Sweden, [2]Department of Physics and Astronomy, Uppsala University, Uppsala, Sweden, [3]IAFE, UBA CONICET, Buenos Aires, Argentina, [4]Department of Physics, FCEyN, UBA, Buenos Aires, Argentina

**Key Points:**

- Electron density spikes of up to ~150 $cm^{-3}$ from RPWS/LP data are observed during the outbound leg of the Cassini's Titan encounters
- The correlation between the density spikes and a decrease of the magnetic field strength is consistent with the presence of a current sheet
- The analysis of 126 encounters reveals the presence of these enhancements in 28 cases

**Correspondence to:**
K. Kim,
konstantin.kim@irfu.se

**Citation:**
Kim, K., Edberg, N. J. T., Shebanits, O., Wahlund, J.-E., Vigren, E., & Bertucci, C. (2023). On current sheets and associated density spikes in Titan's ionosphere as seen from Cassini. *Journal of Geophysical Research: Space Physics*, *128*, e2022JA031118. https://doi.org/10.1029/2022JA031118

Received 28 OCT 2022
Accepted 14 FEB 2023

**Author Contributions:**
**Conceptualization:** Niklas J. T. Edberg
**Formal analysis:** Konstantin Kim
**Funding acquisition:** Niklas J. T. Edberg
**Investigation:** Konstantin Kim, Niklas J. T. Edberg
**Methodology:** Konstantin Kim, Niklas J. T. Edberg, Oleg Shebanits, Jan-Erik Wahlund, Erik Vigren, Cesar Bertucci
**Project Administration:** Niklas J. T. Edberg
**Resources:** Niklas J. T. Edberg
**Software:** Konstantin Kim
**Supervision:** Niklas J. T. Edberg, Jan-Erik Wahlund, Erik Vigren
**Validation:** Konstantin Kim, Oleg Shebanits, Jan-Erik Wahlund, Erik Vigren, Cesar Bertucci
**Visualization:** Konstantin Kim, Oleg Shebanits



**Abstract** The Cassini spacecraft made in-situ measurements of Titan's plasma environment during 126 close encounters between 2004 and 2017. Here we report on observations from the Radio and Plasma Waves System/Langmuir probe instrument (RPWS/LP) from which we have observed, primarily on the outbound leg, a localized increase of the electron density by up to 150 $cm^{-3}$ with respect to the background. This feature, appearing as an electron density spike in the data, is found during 28 of the 126 flybys. The data from RPWS/LP, the electron spectrometer from the Cassini Plasma Spectrometer package , and the magnetometer is used to calculate electron densities and magnetic field characteristics. The location of these structures around Titan with respect to the nominal corotation direction and the sun direction is investigated. We find that the electron density spikes are primarily observed on the dayside and ramside of Titan. We also observe magnetic field signatures that could suggest the presence of current sheets in most cases. The density spikes are extended along the trajectory of the spacecraft with the horizontal scale of ~537 ± 160 km and vertical scale ~399 ± 163 km. We suggest that the density spikes are formed as a result of the current sheet formation.

## 1. Introduction

Titan is one of the largest moons in the Solar system. It has a radius $R_T = 2{,}575$ km, orbiting Saturn within its magnetosphere at a radial distance of 20 Saturn radii (1 $R_S = 60{,}200$ km) with an orbital period of roughly 16 days. Titan possesses a thick and extended atmosphere primarily consisting of $N_2$ and $CH_4$, but with traces of a variety of molecules ranging from molecular hydrogen to complex hydrocarbons and nitriles (Vuitton et al., 2007; Waite et al., 2005). Titan's upper atmosphere is ionized primarily by solar extreme ultraviolet (EUV) radiation, and by energetic electrons and ions from Saturn's magnetosphere. On the dayside solar EUV radiation is the dominant ionization source, for example, Ågren et al. (2009), Vigren et al. (2013), and Shebanits et al. (2013), while the nightside ionosphere is maintained mainly through ionization of neutrals by precipitating magnetospheric electrons, for example, Cravens et al. (2009) and Vigren et al. (2015) and by day-to-night plasma transport (Cui et al., 2010).

The photo- and electron impact ionization of $N_2$ and $CH_4$ leads primarily to the production of $N_2^+$ and $CH_4^+$, but as a result of ion-neutral chemistry, these ion species are rapidly lost and more complex ions are formed. The dominant ion species in Titan's ionosphere are $HCNH^+$ and $C_2H_5^+$ but more complex nitrile and hydrocarbon ions can be combined at least locally to constitute a greater fraction of the ion population (Cravens et al., 2006; Vuitton et al., 2007). As different ion species have different rate constants for undergoing dissociative recombination reactions with free electrons, the ion composition has a direct influence on the overall ionization balance which ultimately dictates the local electron number density. From Cassini flybys, peak dayside electron densities of 2,000–4,000 $cm^{-3}$ are observed typically around altitudes of 1,000–1,300 km, displaying a Chapman-like behavior of the ionosphere. The ionospheric density is decreasing with increasing solar zenith angle (SZA) typically corresponding to a higher peak density located at greater depth (Ågren et al., 2009) and on the nightside the electron density reaches only 1,000 $cm^{-3}$ (Ågren et al., 2009).

While Titan's ionosphere has been studied extensively in the past, primarily using Cassini data, there are still many features left to understand about the dynamics of this complex environment (Galand et al., 2014; Nixon et al., 2018; Wahlund et al., 2014). As a first note, the dynamics of Titan's ionosphere depends heavily on the upstream condition in Saturn's magnetosphere (Bertucci et al., 2009; Edberg et al., 2015; Kabanovic et al., 2017; Simon et al., 2010a, 2010b, 2013). Titan has no signatures of an intrinsic magnetic field, and, therefore, the natural obstacle to the upstream flow is the ionosphere. This interaction leads to a draping of Saturn's magnetospheric

**Writing – original draft:** Konstantin Kim, Niklas J. T. Edberg
**Writing – review & editing:** Konstantin Kim, Niklas J. T. Edberg, Oleg Shebanits, Jan-Erik Wahlund, Erik Vigren

magnetic field lines around Titan, and a weak magnetic pile-up boundary is formed (Ness et al., 1982), similar to that observed at Mars and Venus, for example, Bertucci et al. (2011). The ramside interaction of Titan's plasma environment with Saturn's magnetospheric plasma exhibits a mass-loading process occurring as an ion pick-up. As studied in Sittler et al. (2005), exospheric $CH_4^+$ dominate the pick-up process. The point where the ionosphere is not guiding the escape process—exosphere—is at 4,800 km in the ram direction and 6000 km at the flanks. The pick-up rate was estimated as $5 \times 10^{23}$ ions $s^{-1}$. The mass-loaded magnetic field lines slowly diffuse into the ionosphere over up to several hours, making the induced magnetosphere region a storage for various configurations of upstream magnetic fields. This effect is known as a magnetic memory of Titan's atmosphere (Bertucci et al., 2008) and was first observed during the T32 flyby, when Titan was in the magnetosheath of Saturn. As Saturn's magnetosphere rotates, the corotating magnetospheric plasma hits the ionosphere of Titan from the ramside at sub-magnetosonic speeds of approximately 150 km $s^{-1}$, and there is no bowshock forming at Titan. However, the orbit of Titan (20 $R_S$) is close enough to Saturn's dayside magnetopause ($\simeq$22 $R_S$, Achilleos et al. (2008)), and on some occasions, when Saturn's magnetosphere is externally compressed, Titan can be exposed to the supersonic plasma flow in Saturn's magnetosheath or even to the solar wind (Bertucci et al., 2015; Edberg et al., 2013; Omidi et al., 2017; Penz et al., 2005).

One important mechanism of energy and momentum transfer in planetary atmospheres is the possible formation of a global current system. Such a current system is a common phenomenon in planetary plasma environments and is found to be present on both magnetized (Earth, e.g., Ganushkina et al. (2018)) and unmagnetized bodies (Mars, e.g., Ramstad et al. (2020)), but with somewhat different topology. The ionospheric dynamics and currents are coupled through particle collisions, and one way to evaluate the impact of these on each other is to calculate the electric conductivity of the ionosphere. Currents in Titan's ionosphere have been sparsely investigated in the past. In a study by Rosenqvist et al. (2009), the electrically conductive region of Titan's ionosphere is found at altitudes from 1,000 to 1,450 km. In a subsequent study, using the conductivities from Rosenqvist et al. (2009), Ågren et al. (2011) calculated the current density profiles of Titan's ionosphere for three similar Cassini flybys (T18, T20, and T21). It was found, that there is evidence for horizontal currents of 10–100 $nAm^{-2}$. A recent study revisited Titan's ionospheric conductivities, showing that the negatively charged ions and dust particles increase the Pedersen conductivity by up to 35%, with a few cases of anti-Hall effect (Shebanits et al., 2022).

The aim of this paper is to gain a further understanding of Titan's plasma environment dynamics. We will present observations of hitherto unreported density spikes in Titan's upper ionosphere, seemingly associated with current sheets, which add to the complexity of the system. It is worth mentioning that similar observations of density spikes associated with the current sheet in the topside ionospheric layer were observed by Mars Atmosphere and Volatile Evolution (MAVEN) mission (Kopf et al., 2017) at Mars (see in Discussion).

The paper is structured as follows. In Section 2, we describe the instruments and the data used for the analysis, as well as the methods applied. In Section 3, we start by describing an example of an observation of a density spike, during the T16 encounter, show a number of additional examples, and discuss how we choose the selection criteria for the density spikes. Moreover, we discuss the vertical profile of the measured local magnetic field and its relation to the electron density data. Finally, we discuss the formation and possible causes of the density spikes in Section 4 and summarize the results in Section 5.

## 2. Instrumentation and Methods

### 2.1. RPWS/LP

We use data from the Radio and Plasma Waves System/Langmuir probe (RPWS/LP) to measure the densities of the low-energy population of the ionospheric electrons. RPWS/LP consists of a 5 cm diameter sphere with titanium-nitride (TiN) coating mounted on a tilted 1.5 m boom (Gurnett et al., 2004) separating it 1.28 m from the spacecraft surface. The spatial distancing of the instrument from the spacecraft reduces the influence of the spacecraft charging and emitted photoelectrons. The instrument operates in two different modes: the so-called "20 Hz" mode and in voltage sweep mode. The measurement technique is based on applying a positive or negative bias-voltage on the probe, which then attracts the surrounding thermal plasma, and the resulting current is measured. In the sweep mode during Titan flybys, the applied bias voltage is swept between ±4 V every 24 s for close flybys and ±32 V for distant flybys. When the sphere is charged positively, it will attract multiple populations of thermal electrons, for example, ionospheric electrons, photoelectrons, and possibly secondary

electrons from any particle impacts. Therefore, the positive side of the measured voltage-current curve is used to estimate the electron density and temperature. We also use measurements from the RPWS antenna of the upper-hybrid resonance frequency $f_{UH}$ as a proxy for electron densities. Worth mentioning, the "20 Hz" data are electron temperature dependent. The reduction from Langmuir probe sweeps to the physical properties of density and temperature for various applications have been discussed in several previous papers, for example, Chatain et al. (2021), Gustafsson and Wahlund (2010), Morooka et al. (2011), and Shebanits et al. (2016).

### 2.2. Magnetometer and CAPS

The magnetometer (MAG) onboard Cassini is a fluxgate magnetometer, mounted halfway out an 11 m long boom, to avoid interference with the induced currents from the spacecraft (Dougherty et al., 2004). We use 1 s resolution data to resolve the strength and direction of the local magnetic field. In this study, we will use two different reference frames to represent the magnetic field data and the ephemeris related to the flyby geometry or Titan's position with respect to Saturn.

1. The Titan-centered Titan interaction system (TIIS, also called the Corotational reference frame) where the *X*-axis is parallel to the nominal magnetospheric corotating flow direction, the *Y*-axis points toward Saturn, and the *Z*-axis completes the right-handed system. This is similar to the Kronocentric R, Theta, Phi (KRTP) system but with the following transformations: $X_{TIIS} \rightarrow \Phi$; $Y_{TIIS} \rightarrow -r$; $Z_{TIIS} \rightarrow -\Theta$
2. The Saturn-centered ecliptic frame (SCF) where the *X*-axis points toward the Sun, the *Z*-axis points toward the ecliptic north, and the *Y*-axis completes the right-handed system.

In addition, the Cassini plasma system/electron spectrometer (CAPS/ELS) measures the energy per charge distribution of electrons in the energy range from 0.7 eV to 30 keV and supplements the RPWS/LP observations (Young et al., 2004). Unfortunately, CAPS/ELS ceased to operate in 2012, so this data can only be used for parts of the analysis in this paper.

### 2.3. Minimum Variance Analysis

The minimum variance analysis (MVA/MVAB), described by Sonnerup and Scheible (1998), is used to estimate the direction of the normal vector to current sheets/plasma discontinuities from single-spacecraft measurements. By a normal vector direction to the current sheet surface, the method suggests identifying the direction along which the component of the magnetic field $B_\alpha$ ($\alpha = x, y, z$) has a minimum variance. The direction is found by minimizing the following

$$\sigma^2 = \frac{1}{3}\sum_{\alpha=1}^{3} |(B_\alpha - \langle \mathbf{B} \rangle) \cdot \mathbf{n}|, \quad (1)$$

where $\langle \mathbf{B} \rangle$ is the averaged magnetic field and $B_\alpha$ is the $\alpha$th component of the magnetic field. Equation 1 can be rewritten as an eigenvector and eigenvalue problem $\mathbf{M}_{\beta\gamma} n_\gamma = \lambda n_\beta$ for the variance matrix $\mathbf{M}_{\beta\gamma} = \langle B_\beta B_\gamma \rangle - \langle B_\beta \rangle \langle B_\gamma \rangle$, where $\beta, \gamma = x, y, z$. Solving for $n_\gamma$, a three-component basis in the variance space is calculated and assigned to the maximum (*L*-axis), intermediate (*M*-axis) and minimum (*N*-axis) variances axes, respectively. The variance along the (*L*, *M*, *N*) axis is given by the square root of the corresponding eigenvalue $\lambda$. The *N*-axis (minimum variance axis) is considered the nominal normal direction of the current sheet. The requirement for an accurate detection of the normal direction is that the threshold $\lambda_M/\lambda_N \geq 3$. However, in a study of Knetter et al. (2004), it was shown when calculating the normal direction to discontinuities, that the MVA accuracy primarily depends on the threshold. With an increasing value of a threshold, the accuracy is also increasing. For lower values of this threshold, the accuracy still remains acceptable (within a few tens of degrees) and does not impact the result significantly.

## 3. Observations

Using the measurements of the electron density as described above and analyzing all of the 126 Titan flybys, we observe intermittently occurring density spikes in Titan's upper ionosphere. These have not been investigated previously, even though they are quite substantial in magnitude, duration, and occurrence rate.

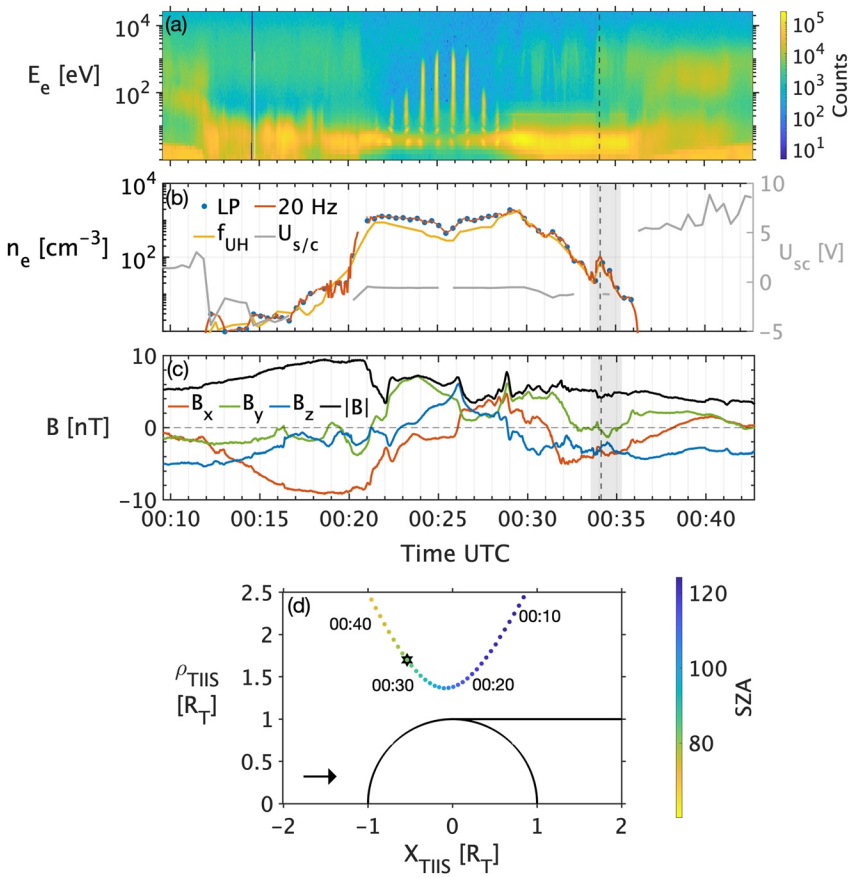


**Figure 1.** The T16 example of an electron density spike with plasma and orbital parameters. (a) The energy-time spectrogram of electrons is measured by CAPS/ELS. The colorbar indicates the counts summed over anodes. (b) The number density of electrons measured by RPWS/LP. The red solid line corresponds to the electron density, derived from $f_{UH}$, the yellow solid line corresponds to electron density from 20 Hz mode, and the blue dots indicate the electron density from RPWS/LP. On the right axis, the spacecraft potential is overlayed (gray solid line). The shaded area and dashed line show the time interval with the density spike. (c) The three components and magnitude of the magnetic field in the TIIS frame. (d) The cylindrical projection of Cassini's trajectory in TIIS coordinate frame with SZA color-coded. The arrow in the bottom left corner shows the nominal direction of plasma flow.

### 3.1. A Density Spike During T16

Figure 1 displays a typical example of the Cassini observation of a density spike during one of its Titan flybys. Figure 1 shows a combined time series plot of RPWS/LP, MAG, and CAPS measurements together with orbital information from the T16 flyby which occurred on 22 July 2006. The electron energy-time spectrogram in Figure 1, panel (a) shows the presence of high-energy magnetospheric electrons (≃1 keV, e.g., 00:35–00:40 UTC) and two populations of low-energy photoelectrons from the ionosphere (≃4 eV, e.g., 00:20–00:22 UTC) and the spacecraft (≃20 eV, e.g., 00:29–00:34 UTC). No signatures of particle acceleration, beam interaction, or intensive thermalization processes are observed at the same time. There is, however, a bite-out of the photoelectron fluxes, indicating a change in the magnetic topology, spacecraft potential, and marking the transition to ionospheric plasma dominant region. The electron density spike, which is of central interest in this paper, can be seen as a distinct, localized enhancement between 00:33 and 00:35 UTC and is shown in panel (b) close to the boundary between ionospheric and magnetospheric plasma. The electron density increases from about 20 to 100 $cm^{-3}$, and is observed only on the outbound leg. This enhancement is observed in $f_{UH}$, LP sweep, and 20 Hz electron density data. Panel (c) shows the three components and the magnitude of the measured magnetic field in the TIIS reference frame. In general, the magnetic field changes direction during the flyby, changing the sign of each component when it is close to Titan. Besides that, in the same time interval (shaded area, panels (b) and (c)) as the density spike, one can find a local change of the $B_y$ component and a local decrease of the total magnetic field. The spacecraft potential is a few volts negative in this interval and increases to positive values just after.

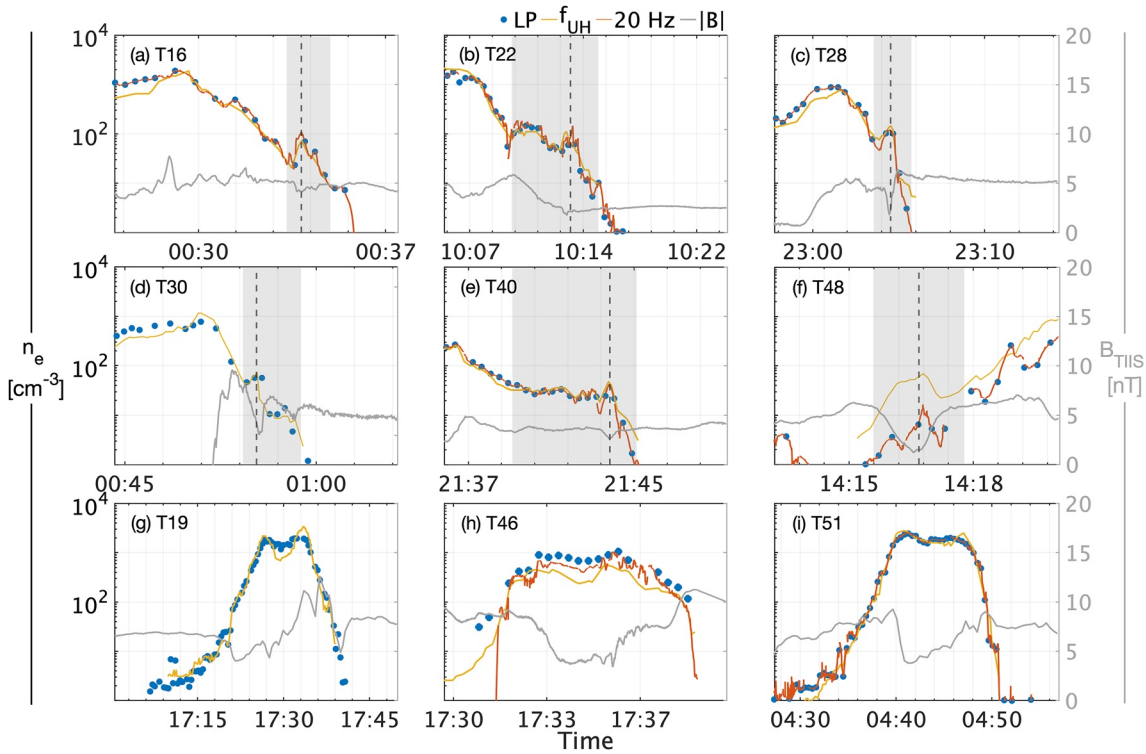


**Figure 2.** Nine examples of density spikes (panels a–f) and three examples (panels g–i) of flybys without spike for comparison as seen from RPWI/LP sweep (blue dots), $f_{UH}$ (solid red line) and "20 Hz" (solid yellow line) data. The total magnetic field is plotted in the same time interval with the scale on the right axis (gray solid line). The shaded area indicates the time interval with the observed electron density enhancements, and the vertical black line indicates the peak density.

This impacts slightly the sampled energies of low energetic electrons and negatively charged particles because the spacecraft itself will repel these charged particles. The electron thermal pressure in the density spike is estimated to $\sim 4 \times 10^{-3}$ nPa, while the same pressure term in the ionosphere varies from $\sim 10^{-4}$ to $\sim 10^{-2}$ nPa. The magnetic pressure throughout the flyby is estimated $\sim 10^{-2}$ nPa and always dominates over the electron thermal pressure. Note that since 2012 CAPS is not measuring electron moments, therefore reliable measurements of low-density electrons are unavailable.

Another important aspect is Cassini's trajectory during Titan encounters. The spacecraft is diving into the atmosphere of Titan down to the ionospheric peak altitude with a speed of $\sim 6$ km s$^{-1}$, covering SZAs from the nightside to the dayside, as shown in Figure 1, panel(d). We use cylindrical projection, such that $\rho = \sqrt{Y^2 + Z^2}$ and X defines the trajectory plane. At the same time, with respect to the corotational direction, Cassini moves from the tailside to the ramside with the closest approach altitude of $\sim 950$ km (see Figure 1, panel (d)). Considering the above observations and the flyby geometry, we define the presence of an enhanced electron density of roughly this magnitude and at roughly this location as the detection criterion for finding more events. The reversal of the magnetic field and the decrease of the total magnetic field seem to be related, and later in the paper, we show that these features are present during most events, although not always.

### 3.2. Density Spikes Throughout the Mission

After searching through all of the 126 Titan encounters, we found 28 cases of density spikes. In Figure 2, we show the electron density as a time series for six additional events, as well as for three flybys when no events are detected, for comparison. As can be seen, the density spikes are not always as clear as during T16 and some appear more like oscillations, as observed during the T22 flyby in Figure 2, panel (b). The amplitude of the density spikes compared to the background values is varying by approximately an order of magnitude in all cases. Notably, there is a decrease in the total magnetic field at the same time interval when the density spikes appear. The magnitude of the magnetic field decreases varies from $\sim 1$ nT (see Figure 2, panels (a, b, e)) to several nT

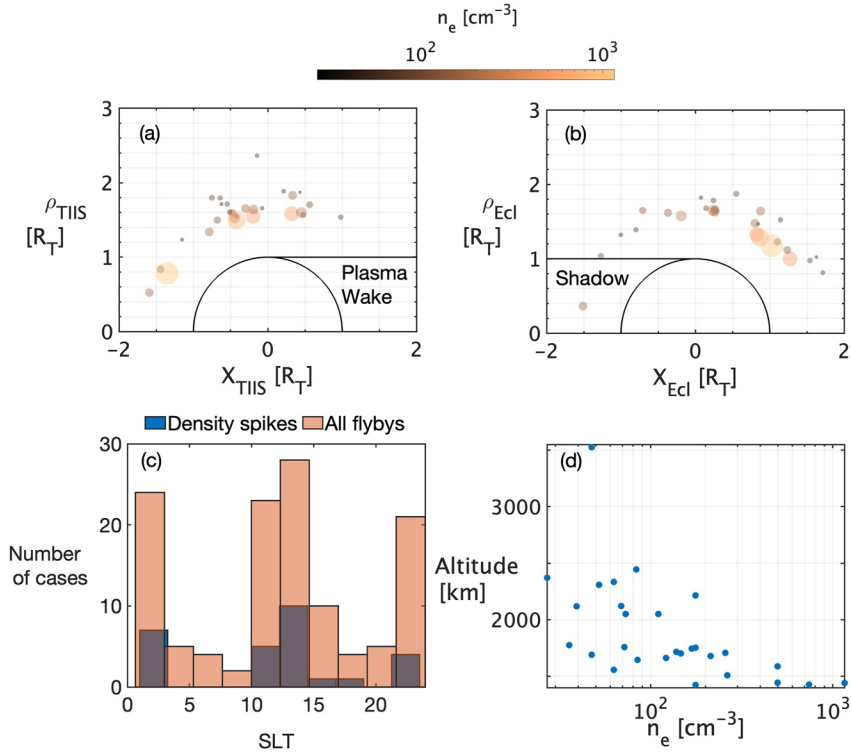


**Figure 3.** Distribution of spikes in (a) corotational (TIIS) and (b) ecliptic coordinates, (c) in Saturn-Centered Ecliptic (i.e., SLT), and (d) the altitude of the spikes versus density. In panels (a) and (b), the color and size of the circles both indicate the electron number density.

(see Figure 2, panels (c, d, f)). Both the decrease of the magnetic field and the electron density enhancement last from several tens of seconds to about 1 min in all cases. The density spikes are observed primarily on the outbound leg, although there are cases (i.e., T48 in panel (f)) when the density spike is observed on the inbound leg of the flyby. In Figure 2, panels (g–i), for comparison, we show some examples from flybys when no density spikes are observed. Although the magnetic field in some cases has local gradients, similarly to the flybys with density spikes, the electron densities show no significant change. In addition, the plasma balance analysis was conducted and showed the dominance of the magnetic pressure term ($\sim 10^{-2}$ nPa) over the thermal pressure term ($\sim 10^{-3}$–$10^{-2}$ nPa) throughout all of the flybys, with an exception in the deep ionosphere.

The distribution of the spikes is plotted in Figure 3 in corotational (a) and ecliptic (b) coordinates. In panel (c), the distribution is shown as a function of Saturn Local Time, and in panel (d), the peak density is plotted versus altitude. The density spikes are generally observed on the ramside of Titan with respect to the direction of the corotating flow, and at the same time, as shown in panels (a–c), the density spikes with higher peak electron density are observed at lower altitudes (panel d). The highest peak values are found on the sunlit side and shown in panel (b). In the Saturn-centered frame (see panel c), the location of the flybys showing density spikes are distributed is not different from the distribution of all of the flybys. Another observation is that the majority of the density spikes are seen on the outbound, which coincidentally is the ramside for most cases, which is discussed below (see Section 4).

Figure 4 shows the vertical profiles of the measured total magnetic field during the Titan encounters, for which we observe density spikes. The magnetic field is normalized so that the maximum magnitude for each case is equal to unity and therefore the absolute values of the magnitude are neglected. We also divide the data by inbound and outbound legs of the trajectory and indicate the altitude where we observe the density spike for each flyby/magnetic profile. The altitudes of the density spikes are scattered around ~1,700 km (0.7 $R_T$) and is shown with the shaded areas indicating a 99% confidence interval of altitudes. From this, we find that an almost coinciding increase in electron density and decrease of the total magnetic field as shown in Figure 4 is present for many other cases, but not all. Note that although the T40 flyby seems to be an outlier in this plot, the

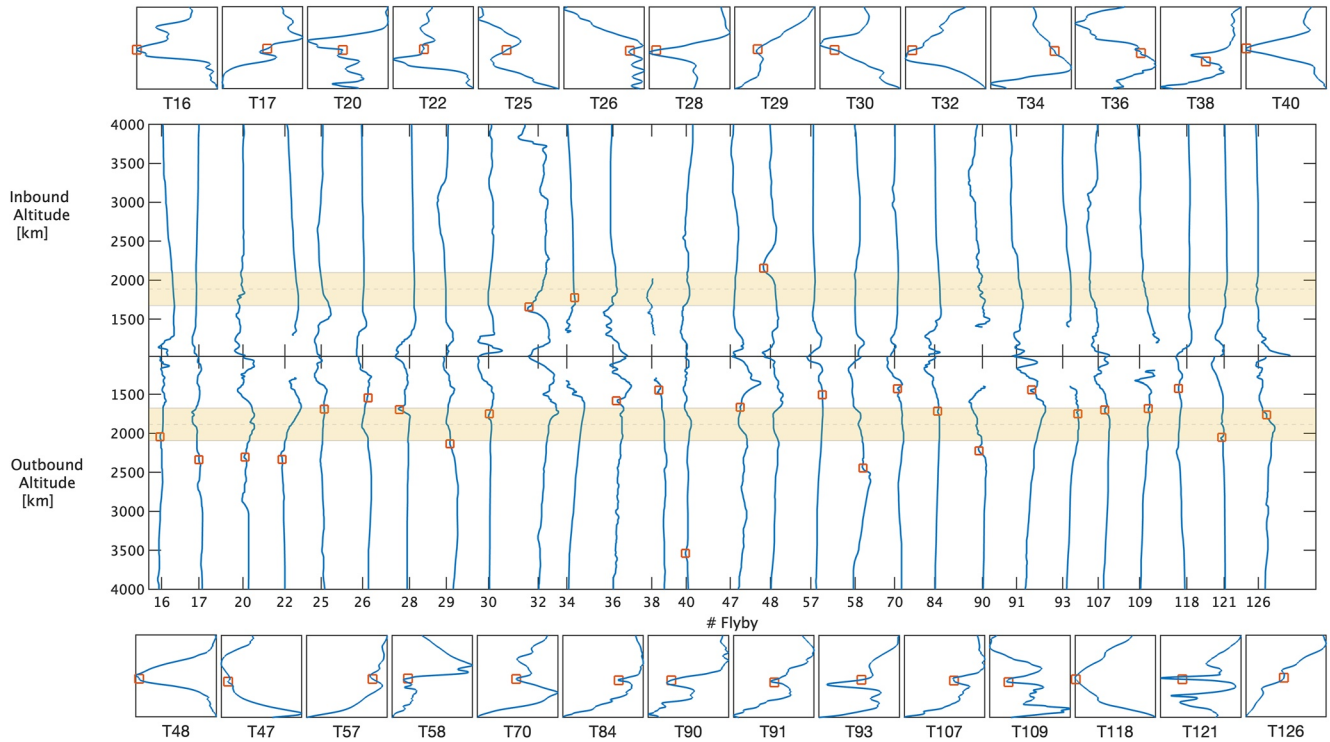


**Figure 4.** Normalized to unity vertical profiles of the magnetic field, divided by inbound and outbound legs. The red squares indicate the altitude when the density spike reaches its peak density. The zoom-ins are showing the location of the peak density events on the normalized to unity magnetic field altitude profiles, indicating that most of them occur during a magnetic field strength dip.

simultaneous decrease of the total magnetic field and electron density enhancement is clearly seen in this case too. Note also that there are magnetic field decreases that are not associated with a density increase, especially so below 1,700 km because of the ionospheric shielding. In addition, the magnetic field dips below 1,700 km might result from the dynamic processes in the ionosphere itself, causing variations in the magnetic field strength as a response to the rapid changes in the upstream magnetic field. Notably, in 12 out of 28 cases, the rotation of the magnetic field is insignificant and there is no decrease in the magnetic field in five cases. In some cases, the peak density of electrons is coinciding with the gradient of a magnetic field, rather than the dip.

In Table 1, the flybys are binned according to the classification of Titan's upstream plasma environment (Kabanovic et al., 2017; Simon et al., 2010a, 2010b). Each row represents gives the median altitude and range of altitudes of a density spike for each group: lobe-lobe (L-L), sheet-lobe (Sh-L/L-Sh) and sheet-sheet (Sh-Sh) transitions. The difference between the median value of altitudes of L-L and Sh-Sh is 17 km, whereas the Sh-L and L-Sh transitions show 392 km difference in median altitude as well as a wider range of altitudes compared to the two other transitions. The analysis of the classification is discussed in detail in Section 4.

**Table 1**
*The Comparison of the Density Spikes Altitudes With Respect to the Upstream Conditions*

| Flyby type | Number of flybys | Median altitude [km] | Range of altitudes [km] |
|---|---|---|---|
| Sh-Sh | 6 | 1,732 | 1,425–2,052 |
| Sh-L | 4 | 1,999 | 1,510–2,373 |
| L-Sh | 4 | 2,391 | 1,557–2,446 |
| L-L | 13 | 1,749 | 1,427–2,217 |

### 3.3. Current Sheets and Density Spikes

A key feature of the observed electron density enhancements seems to be the simultaneous appearance of the local magnetic field gradient and decrease in magnitude, though its decrease in some cases is insignificant. However, a decrease in the local magnetic field strength accompanied by a field rotation indicates a presence of an electric current in this area.

If we assume that these rotations are indeed due to electric currents, from minimum variance analysis of magnetic field (MVAB) we can retrieve normal vectors to the current sheet surface. The magnetic field components are therefore transformed into MVAB reference frame, which is essentially the (*L,M,N*) basis. For example, in Figure 5, panels (c,d) we show the results

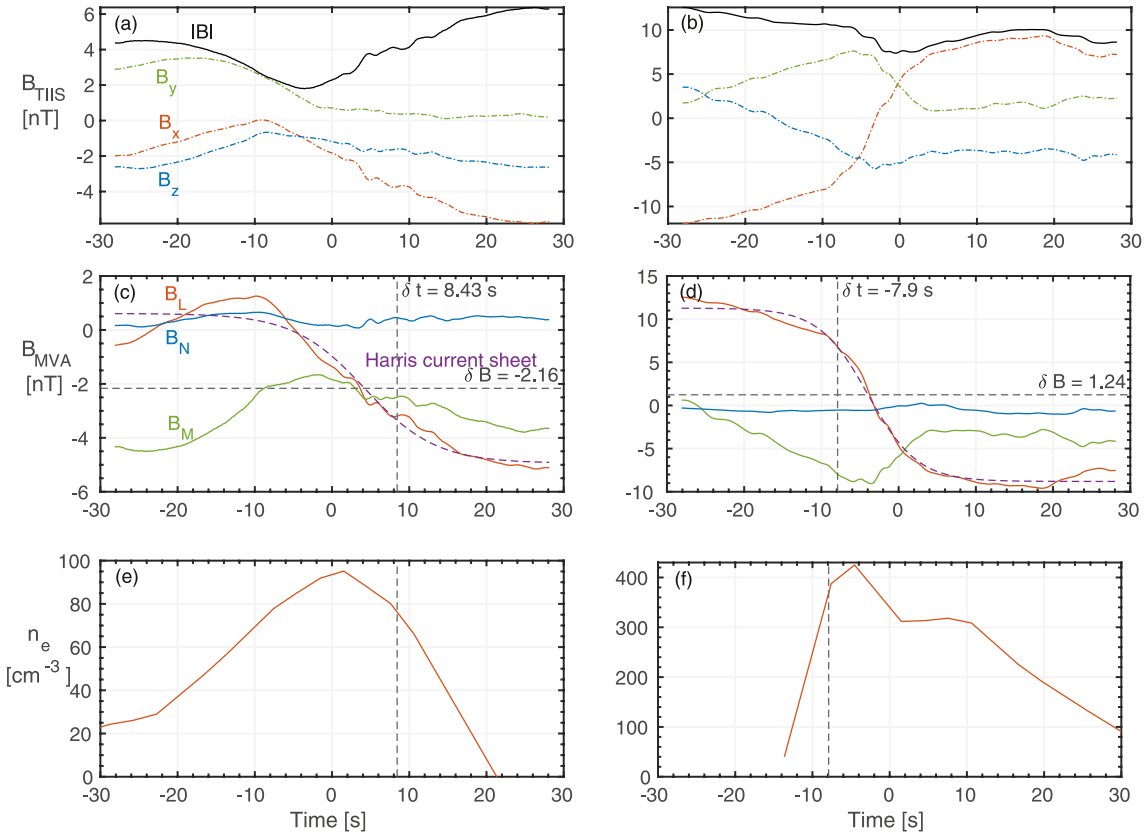


**Figure 5.** An example of minimum variance analysis method for T28 and T36 flyby. All the data are centered around the peak electron density. Panels (a), (b) show the components (dashed lines) and magnitude of the magnetic field; panels (c), (d) show the maximum ($B_L$), intermediate ($B_M$) and minimum ($B_N$) variance components of the magnetic field (solid lines), and the purple line shows the fit from Equation 2, while the dashed horizontal lines show the offsets; panels (e), (f) show the number density of electrons (red line) with subtracted background electron density.

of the MVAB for the T28 and T36 flyby. The magnetic field components in MVAB frame and the electron density above the background are plotted with respect to the time of the assumed current sheet crossing. The maximum variance component $B_L$ is fitted with a modified Harris-current sheet model

$$B_L = \delta B + B_0 \tanh\left(\frac{t+\delta t}{T}\right), \tag{2}$$

where $\delta B$, $B_0$, $\delta t$, $T$ are the fitting parameters. In this example, the maximum variance component $B_L$ changes its sign and magnitude during the crossing. The fitted model of a Harris current sheet (Equation 2) shows consistency with the data. The time offset is present due to the manual selection of the current sheet time crossing. However, the $\delta t$ offset is negligible compared to the total time of the current sheet crossing.

In Figure 5, panels (e, f), the measured electron density profile with subtracted background density is shown. The peak of the electron density corresponds to the breaking point (change of sign) of the $B_L$ component of the magnetic field, which is consistent with the Harris current sheet model. The peak values of the electron density for T28 and T36 reach a value slightly above 100 and 400 $cm^{-3}$, respectively. This technique is applicable for indicating Harris-type current sheet, which has recently been done at for instance Mars, see Grigorenko et al. (2019). The same procedure is applied to the rest of the events found in this study. As described in Section 2.3, the normal vector to the current sheet surface is calculated as a minimum variance axis. The normal vector direction is valid if $\lambda_M/\lambda_N \geq 3$. In four cases this, relation is below 2, and for the rest of them, this value is well above 3. In Figure 6, panel (a), shows the normal vectors with respect to Titan in cylindrical coordinates, excluding the cases which do not satisfy the eigenvalue condition.

We calculate the angle between the normal to the current sheet and the radial direction, and color-coded in Figure 6, panel (a). There are 18 cases with the angle $\leq 45°$, with values of $\sim 22.3 \pm 12.4°$. The normal vectors are

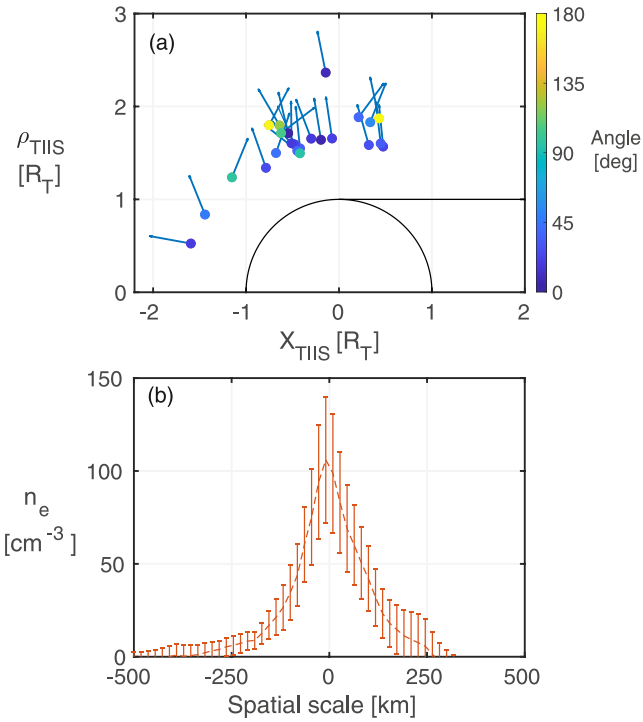


**Figure 6.** The results of MVA method for all cases together with the density measurements: in panel (a), the orientation of the magnetic normal vectors to the assumed current sheet surface are shown projected onto the cylindrical frame; in panel (b), the mean number density of electrons density spikes with subtracted background density, averaged over all cases, is shown.

primarily oriented radially outward from Titan, forming a consistent current sheet layer structure. In the lower panel (b) we show the mean values of the density for all found density spikes. It is shown how the electron density profile depends on the time from the assumed current sheet crossing. The average value of the peak density reaches slightly above 100 $cm^{-3}$. The spatial scale of the density spikes is estimated as the full width at half maximum (FWHM) and is approximately 200–250 km, meaning about 500 km in the along-track direction. The more accurate estimation of the vertical and horizontal scales corresponds to ∼399 ± 163 km and ∼537 ± 160 km, respectively.

We estimate the current density $J$ by using Ampere's law in the vicinity of the electron density spikes

$$\nabla \times \mathbf{B} = \mu_0 \mathbf{J} \rightarrow J \simeq \frac{\Delta B}{\mu_0 \Delta L}, \quad (3)$$

where B is the magnetic field magnitude, L is the altitude, and $\mu_0$ is magnetic permeability. The estimated median value of the current density J ≃ 2.75 $nAm^{-2}$ but spanning values in the range from a minimum 0.16 $nAm^{-2}$ up to a maximum of 17.8 $nAm^{-2}$.

## 4. Discussion

The observed density spikes appear in 28 out of 126 flybys. In the Saturn-centered frame, the distribution of the cases follows the distribution of the flyby positions (see Figure 3, panel (c)). That tells us that the density spikes do not favor any particular region of Saturn's magnetosphere. The altitudes of the density spikes range from 1,280 km up to 2,570 km (or from ∼0.5–1 $R_T$), if neglecting the T40 outlier, with an average altitude of 1,700 km (or 0.7 $R_T$), which is on average higher than the exobase of Titan, located at 1,450 km. Only ∼78% (∼68%) of all of the flybys reaches a minimum altitude of less than ∼2,540 km (∼1,800) km, respectively. From this, we infer that the occurrence rate of the density spikes is around 28/(0.78 (0.68)*126) = 28–33%. The observed cases occur primarily on the ramside of Titan, suggesting that the density spikes are likely related to the interaction between the upstream plasma environment of Saturn and Titan's upper ionosphere.

There is a clear correlation between the presence of the density spikes and the local gradient and rotation of the magnetic field. The diversity of density spikes shown in Figure 2 reveals the variations in the magnitude of magnetic field decrease and electron density enhancement. However, there are no particular CAPS/ELS observations in this region that stand out, which otherwise could have been indicating particle acceleration, plasma heating, or increased impact ionization.

As a next step, we wish to understand the underlying physical process leading to the formation of the density spikes. Based on the features described earlier, we formulate the following hypothesis on the origin of these structures.

1. Current sheets in the topside ionosphere, induced by upstream magnetospheric flows.
2. Outflow of detached plasma structures.

Since there is a high variability in Saturn's magnetospheric plasma conditions upstream of Titan the magnetic field orientation can change rapidly. As the magnetic field is slowed down and draped around Titan while it slowly diffuses through the system, field lines with different topologies could pile up. The changes in the magnetic field topology lead to the generation of local currents, according to Ampere's law; therefore, one should expect the presence of currents in the vicinity of field rotation regions. Further discussion is held under the assumption that the time and spatial scales of a density spike are larger than the ion scales in the vicinity of Titan, thus the dynamics of the magnetic fields is treated in the magnetohydrodynamics sense.

To investigate the origin of the current sheet, we consider the observed rotations and dips in the magnetic field, an increase in the electron density, and the altitude of the observations. In the paper of Ågren et al. (2011), the currents above the exobase (∼1,450 km) are assumed to be present as a result of Saturn's magnetosphere interaction with Titan's ionosphere. The magnetic field lines diffuse into Titan's ionosphere at altitudes from ∼1,150 to 2,440 km on the dayside magnetosphere of Saturn, and from ∼1,150 to 2,180 km on the nightside region (Chen & Simon, 2020). In the boundary layer where the thermal pressure of the ionosphere balances the magnetic pressure of the diffused field lines, which would be known as the ionopause (although a proper ionopause has not really been observed at Titan), the shielding currents are formed as a response to the changes in the magnetic field configuration. Using the classification of upstream conditions (Simon et al., 2010a, 2010b; Kabanovic et al., 2017), we find that the flybys density spikes at the lower than average altitudes are generally those that are exposed to the plasma sheet. The plasma sheet would cause an increase in the upstream plasma pressure compared to the upstream plasma pressure in the lobe regions. For that reason, the density spikes themselves can be interpreted as a crossing of the plasma compression region between the ionosphere and the pile-up region with the presence of shielding currents, caused by the draping process. We can therefore interpret the signatures reported in this paper as if they were ionopause crossings. The altitude of this ionopause-like boundary varies with changes in the upstream conditions, thus rapid changes in the position are expected. For example, in the observations of cold ionospheric plasma during the TA flyby (Wahlund et al., 2005), the ionopause has changed altitude on the time scale of going from the inbound to the outbound leg.

A nested current sheet is another mechanism to describe the origin of observed current sheets. This mechanism was proposed by Volwerk et al. (2017) to occur around the comet 67P/Churyumov-Gerasimenko. The described process appears as a response to the changes in upstream conditions in the solar wind and further layering during the pileup of magnetic field lines on the ramside of the cometary coma. The same signatures of a local decrease in the magnetic field strength and an enhancement of the electron density would be observed in such a case. This might be possible due to the presence of the "magnetic memory" or "fossil magnetic fields" in Titan's plasma environment (Bertucci et al., 2008). Though one should consider that during the T32 flyby, Titan was exposed to Saturn's magnetosheath and shocked solar wind plasma. The heavily mass-loaded magnetic field lines slowly diffuse into the ionosphere within several hours making the induced magnetosphere region store various configurations of upstream magnetic fields. With the high variability of the upstream conditions and the ability of the induced magnetosphere region to memorize the previous states of the upstream magnetic field, the interaction of two layers with conflicting orientations of the magnetic field is expected. Thus, if the region between these two layers is compressed, it might cause a local increase in the electron density. Such interaction would also explain the presence of the density spikes without the signatures of a significant magnetic field rotation—in case of an interaction between two layers with slightly different orientations of the magnetic field. The diffusion time is large enough compared to the flyby time, therefore it is possible to capture this transient effect during one flyby. The layering around certain altitudes of the detected density spikes is explained by the draping geometry of the magnetic field lines which remains the same for different field configurations.

An outflow of detached plasma structures is another candidate for the origins of the density spikes. Detached plasma structures can be formed as a result of a shear instability developing between the upstream plasma flow and ionosphere, and leading to a loss of ionospheric plasma. If this is what would have been observed, the detached plasma structures would have increased the densities of cold electrons and ions as well as the magnetic field strength, which contradicts the observations. One should keep in mind that there are no CAPS measurements since 2012. In addition, if there is a current sheet in the outer boundary of such a structure, one would expect to see a random distribution of normal directions, rather than the observed radially outward orientation.

Finally, we examined the changes in the neutral atmosphere composition by the analysis of INMS data. The vertical profiles of neutral species are measured up to 900 km above the surface of Titan, and no significant signatures of any change in the neutral atmospheric composition were found. There are no obvious signatures of increased fluxes of neutral particles occurring in these instances either. One should also note that any dynamical process in Titan's atmosphere, for example, neutral winds or general circulation and convection, at this altitude should be neglected. The shielding currents and nested currents mechanisms fit the observation to some extent. Although the observed events are consistent with current sheets, not all of the cases have explicit rotation signatures. This might give the impression that the density spike appears due to another nonlinear process, which results in the local gradients of the magnetic field. This unknown process is a possible direction for further research. According to Chen and Simon (2020), the strength of a piled-up magnetic field never drops to zero. Nevertheless, it starts to

weaken at around ~900 km (0.35 $R_T$), which can be assigned to the average position of an ionopause. The average altitude of the density spikes is ~1,700 km (0.7 $R_T$) which is twice as big as the ionopause position estimation, while the range of altitudes of the density spikes is consistent with the piled-up region estimates of Chen and Simon (2020). The differences in these two estimations are probably caused by the insensitivity for variations of upstream conditions collected below 1,600 km due to the influence of fossil fields (Bertucci et al., 2008). It is also quite interesting that even though it is believed that the magnetic pressure in the plasma sheet region (Sh-Sh) is larger than in the lobes (L-L) (see the comparison in our data set from Table 1) an insignificant difference between them is displayed. Even though the difference is small between these two groups most likely because of a low number of cases, the difference in altitude between Sh-L\L-Sh and L-L\Sh-Sh transitions is significant. Another limitation is the selection criteria, which is based on the presence of the density spikes in the measurements from the RPWS/LP and also from the $f_{UH}$. The reason why density profiles from RPWS/LP, unlike profiles from $f_{UH}$, do not show the density spikes might be because of the differences in time resolution of the measurements. As for the nested current sheets, the main disadvantage of this mechanism is that it does not fit the aforementioned classification. During the Sh-Sh transitions most likely one expects to see the density spike at the lower altitudes compared to Sh-L and L-L transitions, which is partially true. In fact, less than half of the cases satisfy this criterion, and the median density spike altitude during L-L transitions is almost the same as Sh-Sh.

The absence of these structures in all of the flybys should also be addressed. Indeed, the proposed mechanism is similar to the nested current sheets, and in combination with the fossilized fields might lock the changes in the system on a characteristic time, therefore the density spikes could appear in every flyby, which is not observed. We don't have a clear explanation of such a scenario. The possible explanation is that the evolved current sheet has an uneven geometry and appears locally in the vicinity of the most rapid changes in the upstream region. Given that, the majority of cases are observed on the ramside (see Figure 3a) and taking into account that some of the flybys are not crossing the ramside during a sufficient amount of time, the probability of observing the density spike is decreasing. This feature can explain why density spikes appear only in a limited fraction of flybys. Another option is that not during all of the flybys Titan's plasma environment was experiencing global changes in the magnetic field and plasma properties in the upstream region which would then not result in any dynamical features in the ionosphere.

As was already mentioned in the Introduction, similar density spikes were observed at Mars by MAVEN (Kopf et al., 2017). The increase in electron and ion densities is accompanied by a rotation and decrease in the magnetic field. Various possible explanations are proposed by Kopf et al. (2017), among those are magnetic reconnection, shear instability, magnetic flux ropes and current sheet crossing. These interpretations are also applicable in the case of Titan but with a few corrections. First, Mars is exposed directly to the supersonic solar wind, which transfers the frozen-in interplanetary magnetic field, while Titan is embedded into Saturn's magnetosphere, which most of the time shields it from the solar wind and Saturn's magnetosheath plasma. Second, Mars has crustal magnetic fields in the southern hemisphere, which causes the asymmetry in the configuration of the plasma environment, while Titan has no intrinsic magnetic field (Backes et al., 2005). Otherwise, the general interaction patterns are similar, which involve pile-up and draping of the magnetic field, and current generation.

## 5. Conclusions

To summarize, we observe electron density enhancements, or density spikes, in Titan's topside ionosphere at altitudes of approximately 1,700 km, using the Cassini spacecraft. The magnitude of the peak electron density is roughly below 150 $cm^{-3}$ on average, but significantly above the background electron density. A common feature of the observed electron density spikes is the coincident rotation and decrease of the local magnetic field. We found 28 similar cases of density spikes in the overall 126 flybys. The density spikes are located primarily on the ramside of Titan, forming an apparent layer of ~399 ± 163 km thickness. The current density estimation shows the presence of a current in the range from 0.16 to 17.8 $nAm^{-2}$, which is lower than the calculated by Ågren et al. (2011) values for the currents at altitudes below the exobase.

The formation of a current sheet on the ramside of Titan gives the best explanation to the measurements within the described properties of the observed plasma structures. We propose that the currents are driven by the rapid changes in upstream conditions and the draping of the magnetic field lines with further mass-loading and diffusion into the ionosphere. These currents have similarities with shielding currents in the ionopause, which balance the upstream magnetic pressure with the thermal pressure of the ionosphere and nested current sheets, resulting

from the layering of the upstream magnetic field. In both cases, the density spikes appear in the compression region either between the ionosphere and diffused upstream magnetic field, or between two layers of different magnetic field configurations. An important aspect of Titan's ionosphere is the magnetic memory, which makes it possible to store the state of the upstream magnetic field. Therefore, the density spike is identified as a compressed ionospheric plasma, corresponding to the transient changes in the magnetic field configuration.

## Data Availability Statement

All the data used in this study is available on the Planetary Data System/NASA on the Cassini RPWS, MAG and CAPS subpages (https://pds-ppi.igpp.ucla.edu/).

**Acknowledgments**
Konstantin Kim and Niklas J. T. Edberg acknowledge funding from the Swedish Research Council (Vetenskapsrådet) under contract 2020-03962. SNSA (formerly SNSB) supported the RPWS/LP instrument onboard Cassini.

## References

Achilleos, N., Arridge, C. S., Bertucci, C., Jackman, C. M., Dougherty, M. K., Khurana, K. K., & Russell, C. T. (2008). Large-scale dynamics of Saturn's magnetopause: Observations by Cassini. *Journal of Geophysical Research (Space Physics)*, *113*(A11), A11209. https://doi.org/10.1029/2008JA013265

Ågren, K., Andrews, D. J., Buchert, S. C., Coates, A. J., Cowley, S. W. H., Dougherty, M. K., et al. (2011). Detection of currents and associated electric fields in Titan's ionosphere from Cassini data. *Journal of Geophysical Research (Space Physics)*, *116*(A4), A04313. https://doi.org/10.1029/2010JA016100

Ågren, K., Wahlund, J.-E., Garnier, P., Modolo, R., Cui, J., Galand, M., & Müller-Wodarg, I. (2009). On the ionospheric structure of titan. *Planetary and Space Science*, *57*(14), 1821–1827. https://doi.org/10.1016/j.pss.2009.04.012

Backes, H., Neubauer, F. M., Dougherty, M. K., Achilleos, N., André, N., Arridge, C. S., et al. (2005). Titan's magnetic field signature during the first Cassini encounter. *Science*, *308*(5724), 992–995. https://doi.org/10.1126/science.1109763

Bertucci, C., Achilleos, N., Dougherty, M. K., Modolo, R., Coates, A. J., Szego, K., et al. (2008). The magnetic memory of titan's ionized atmosphere. *Science*, *321*(5895), 1475–1478. https://doi.org/10.1126/science.1159780

Bertucci, C., Duru, F., Edberg, N., Fraenz, M., Martinecz, C., Szego, K., & Vaisberg, O. (2011). The induced magnetospheres of Mars, Venus, and titan. *Space Science Reviews*, *162*(1–4), 113–171. https://doi.org/10.1007/s11214-011-9845-1

Bertucci, C., Hamilton, D. C., Kurth, W. S., Hospodarsky, G., Mitchell, D., Sergis, N., et al. (2015). Titan's interaction with the supersonic solar wind. *Geophysical Research Letters*, *42*(2), 193–200. https://doi.org/10.1002/2014GL062106

Bertucci, C., Sinclair, B., Achilleos, N., Hunt, P., Dougherty, M. K., & Arridge, C. S. (2009). The variability of Titan's magnetic environment. *Planetary and Space Science*, *57*(14–15), 1813–1820. https://doi.org/10.1016/j.pss.2009.02.009

Chatain, A., Wahlund, J. E., Shebanits, O., Hadid, L. Z., Morooka, M., Edberg, N. J. T., et al. (2021). Re-analysis of the Cassini RPWS/LP data in titan's ionosphere: 1. Detection of several electron populations. *Journal of Geophysical Research (Space Physics)*, *126*(8), e28412. https://doi.org/10.1029/2020JA028412

Chen, C., & Simon, S. (2020). A comprehensive study of Titan's magnetic pile-up region during the Cassini era. *Planetary and Space Science*, *191*, 105037. https://doi.org/10.1016/j.pss.2020.105037

Cravens, T. E., Robertson, I. P., Waite, J. H., Yelle, R. V., Kasprzak, W. T., Keller, C. N., et al. (2006). Composition of Titan's ionosphere. *Geophysical Research Letters*, *33*(7), L07105. https://doi.org/10.1029/2005GL025575

Cravens, T. E., Robertson, I. P., Waite, J. H., Yelle, R. V., Vuitton, V., Coates, A. J., et al. (2009). Model-data comparisons for Titan's nightside ionosphere. *Icarus*, *199*(1), 174–188. https://doi.org/10.1016/j.icarus.2008.09.005

Cui, J., Galand, M., Yelle, R. V., Wahlund, J.-E., Ågren, K., Waite, J. H., Jr., & Dougherty, M. K. (2010). Ion transport in titan's upper atmosphere. *Journal of Geophysical Research*, *115*(A6). https://doi.org/10.1029/2009JA014563

Dougherty, M. K., Kellock, S., Southwood, D. J., Balogh, A., Smith, E. J., Tsurutani, B. T., et al. (2004). The Cassini magnetic field investigation. *Space Science Reviews*, *114*(1–4), 331–383. https://doi.org/10.1007/s11214-004-1432-2

Edberg, N. J. T., Andrews, D. J., Bertucci, C., Gurnett, D. A., Holmberg, M. K. G., Jackman, C. M., et al. (2015). Effects of Saturn's magnetospheric dynamics on Titan's ionosphere. *Journal of Geophysical Research (Space Physics)*, *120*(10), 8884–8898. https://doi.org/10.1002/2015JA021373

Edberg, N. J. T., Andrews, D. J., Shebanits, O., Ågren, K., Wahlund, J. E., Opgenoorth, H. J., et al. (2013). Extreme densities in Titan's ionosphere during the T85 magnetosheath encounter. *Geophysical Research Letters*, *40*(12), 2879–2883. https://doi.org/10.1002/grl.50579

Galand, M., Coates, A. J., Cravens, T. E., & Wahlund, J.-E. (2014). Titan's ionosphere. In I. Müller-Wodarg, C. A. Griffith, E. Lellouch, & T. E. Cravens (Eds.), *Titan: Interior, surface, atmosphere, and space environment* (pp. 376–418). Cambridge University Press. https://doi.org/10.1017/CBO9780511667398.014

Ganushkina, N. Y., Liemohn, M. W., & Dubyagin, S. (2018). Current systems in the earth's magnetosphere. *Reviews of Geophysics*, *56*(2), 309–332. https://doi.org/10.1002/2017RG000590

Grigorenko, E. E., Zelenyi, L. M., DiBraccio, G., Ermakov, V. N., Shuvalov, S. D., Malova, H. V., et al. (2019). Thin current sheets of sub-ion scales observed by MAVEN in the martian magnetotail. *Geophysical Research Letters*, *46*(12), 6214–6222. https://doi.org/10.1029/2019GL082709

Gurnett, D. A., Kurth, W. S., Kirchner, D. L., Hospodarsky, G. B., Averkamp, T. F., Zarka, P., et al. (2004). The Cassini Radio and plasma Wave investigation. *Space Science Reviews*, *114*(1–4), 395–463. https://doi.org/10.1007/s11214-004-1434-0

Gustafsson, G., & Wahlund, J. E. (2010). Electron temperatures in Saturn's plasma disc. *Planetary and Space Science*, *58*(7–8), 1018–1025. https://doi.org/10.1016/j.pss.2010.03.007

Kabanovic, S., Simon, S., Neubauer, F. M., & Meeks, Z. (2017). An empirical model of titan's magnetic environment during the Cassini era: Evidence for seasonal variability. *Journal of Geophysical Research (Space Physics)*, *122*(11), 11076–11085. https://doi.org/10.1002/2017JA024402

Knetter, T., Neubauer, F. M., Horbury, T., & Balogh, A. (2004). Four-point discontinuity observations using cluster magnetic field data: A statistical survey. *Journal of Geophysical Research (Space Physics)*, *109*(A6), A06102. https://doi.org/10.1029/2003JA010099

Kopf, A. J., Gurnett, D. A., DiBraccio, G. A., Morgan, D. D., & Halekas, J. S. (2017). The transient topside layer and associated current sheet in the ionosphere of Mars. *Journal of Geophysical Research (Space Physics)*, *122*(5), 5579–5590. https://doi.org/10.1002/2016JA023591

Morooka, M. W., Wahlund, J. E., Eriksson, A. I., Farrell, W. M., Gurnett, D. A., Kurth, W. S., et al. (2011). Dusty plasma in the vicinity of Enceladus. *Journal of Geophysical Research (Space Physics)*, *116*(A12), A12221. https://doi.org/10.1029/2011JA017038

Ness, N. F., Acuna, M. H., Behannon, K. W., & Neubauer, F. M. (1982). The induced magnetosphere of Titan. *Journal of Geophysical Research (Space Physics)*, *87*(A3), 1369–1382. https://doi.org/10.1029/JA087iA03p01369

Nixon, C. A., Lorenz, R. D., Achterberg, R. K., Buch, A., Coll, P., Clark, R. N., et al. (2018). Titan's cold case files - Outstanding questions after Cassini-Huygens. *Planetary and Space Science*, *155*, 50–72. https://doi.org/10.1016/j.pss.2018.02.009

Omidi, N., Sulaiman, A. H., Kurth, W., Madanian, H., Cravens, T., Sergis, N., et al. (2017). A single deformed bow shock for titan-Saturn system. *Journal of Geophysical Research (Space Physics)*, *122*(11), 11058–11075. https://doi.org/10.1002/2017JA024672

Penz, T., Lammer, H., Kulikov, Y. N., & Biernat, H. K. (2005). The influence of the solar particle and radiation environment on Titan's atmosphere evolution. *Advances in Space Research*, *36*(2), 241–250. https://doi.org/10.1016/j.asr.2005.03.043

Ramstad, R., Brain, D. A., Dong, Y., Espley, J., Halekas, J., & Jakosky, B. (2020). The global current systems of the Martian induced magnetosphere. *Nature Astronomy*, *4*(10), 979–985. https://doi.org/10.1038/s41550-020-1099-y

Rosenqvist, L., Wahlund, J. E., Ågren, K., Modolo, R., Opgenoorth, H. J., Strobel, D., et al. (2009). Titan ionospheric conductivities from Cassini measurements. *Planetary and Space Science*, *57*(14–15), 1828–1833. https://doi.org/10.1016/j.pss.2009.01.007

Shebanits, O., Wahlund, J. E., Edberg, N. J. T., Crary, F. J., Wellbrock, A., Andrews, D. J., et al. (2016). Ion and aerosol precursor densities in titan's ionosphere: A multi-instrument case study. *Journal of Geophysical Research (Space Physics)*, *121*(10). https://doi.org/10.1002/2016JA022980

Shebanits, O., Wahlund, J. E., Mandt, K., Ågren, K., Edberg, N. J. T., & Waite, J. H. (2013). Negative ion densities in the ionosphere of Titan-Cassini RPWS/LP results. *Planetary and Space Science*, *84*, 153–162. https://doi.org/10.1016/j.pss.2013.05.021

Shebanits, O., Wahlund, J.-E., Waite, J. H., & Dougherty, M. K. (2022). Conductivities of titan's dusty ionosphere. *Journal of Geophysical Research: Space Physics*, *127*(2), e2021JA029910. https://doi.org/10.1029/2021JA029910

Simon, S., Treeck, S. C., Wennmacher, A., Saur, J., Neubauer, F. M., Bertucci, C. L., & Dougherty, M. K. (2013). Structure of Titan's induced magnetosphere under varying background magnetic field conditions: Survey of Cassini magnetometer data from flybys TA-T85. *Journal of Geophysical Research (Space Physics)*, *118*(4), 1679–1699. https://doi.org/10.1002/jgra.50096

Simon, S., Wennmacher, A., Neubauer, F. M., Bertucci, C. L., Kriegel, H., Russell, C. T., & Dougherty, M. K. (2010a). Dynamics of Saturn's magnetodisk near Titan's orbit: Comparison of Cassini magnetometer observations from real and virtual Titan flybys. *Planetary and Space Science*, *58*(12), 1625–1635. https://doi.org/10.1016/j.pss.2010.08.006

Simon, S., Wennmacher, A., Neubauer, F. M., Bertucci, C. L., Kriegel, H., Saur, J., et al. (2010b). Titan's highly dynamic magnetic environment: A systematic survey of Cassini magnetometer observations from flybys TA-T62. *Planetary and Space Science*, *58*(10), 1230–1251. https://doi.org/10.1016/j.pss.2010.04.021

Sittler, E. C., Hartle, R. E., ViñAs, A. F., Johnson, R. E., Smith, H. T., & Mueller-Wodarg, I. (2005). Titan interaction with Saturn's magnetosphere: Voyager 1 results revisited. *Journal of Geophysical Research (Space Physics)*, *110*(A9), A09302. https://doi.org/10.1029/2004JA010759

Sonnerup, B. U. Ö., & Scheible, M. (1998). Minimum and maximum variance analysis. *ISSI Scientific Reports Series*, *1*, 185–220.

Vigren, E., Galand, M., Yelle, R. V., Cui, J., Wahlund, J. E., Ågren, K., et al. (2013). On the thermal electron balance in Titan's sunlit upper atmosphere. *Icarus*, *223*(1), 234–251. https://doi.org/10.1016/j.icarus.2012.12.010

Vigren, E., Galand, M., Yelle, R. V., Wellbrock, A., Coates, A. J., Snowden, D., et al. (2015). Ionization balance in Titan's nightside ionosphere. *Icarus*, *248*, 539–546. https://doi.org/10.1016/j.icarus.2014.11.012

Volwerk, M., Jones, G. H., Broiles, T., Burch, J., Carr, C., Coates, A. J., et al. (2017). Current sheets in comet 67P/Churyumov-Gerasimenko's coma. *Journal of Geophysical Research (Space Physics)*, *122*(3), 3308–3321. https://doi.org/10.1002/2017JA023861

Vuitton, V., Yelle, R. V., & McEwan, M. J. (2007). Ion chemistry and N-containing molecules in Titan's upper atmosphere. *Icarus*, *191*(2), 722–742. https://doi.org/10.1016/j.icarus.2007.06.023

Wahlund, J. E., Boström, R., Gustafsson, G., Gurnett, D. A., Kurth, W. S., Pedersen, A., et al. (2005). Cassini measurements of cold plasma in the ionosphere of titan. *Science*, *308*(5724), 986–989. https://doi.org/10.1126/science.1109807

Wahlund, J. E., Modolo, R., Bertucci, C., & Coates, A. J. (2014). Titan's magnetospheric and plasma environment. In *Titan*. https://doi.org/10.1017/CBO9780511667398.015.419

Waite, J. H., Niemann, H., Yelle, R. V., Kasprzak, W. T., Cravens, T. E., Luhmann, J. G., et al. (2005). Ion neutral mass spectrometer results from the first flyby of titan. *Science*, *308*(5724), 982–986. https://doi.org/10.1126/science.1110652

Young, D. T., Berthelier, J. J., Blanc, M., Burch, J. L., Coates, A. J., Goldstein, R., et al. (2004). Cassini plasma spectrometer investigation. *Space Science Reviews*, *114*(1–4), 1–112. https://doi.org/10.1007/s11214-004-1406-4